Electro-optically induced absorption in α-Si:H/α-SiCN waveguiding multistacks

Francesco G. Della Corte,[1] Sandro Rao,[1*] Maria A. Nigro,[1] Francesco Suriano,[1] Caterina Summonte[2]

[1]*Department of Information Science, Mathematics, Electronics and Transportations (DIMET)*
"Mediterranea" University, Via Graziella Località Feo di Vito
I-89060, Reggio Calabria, Italy
[2]*Institute for Microelectronics and Microsystems – Consiglio Nazionale delle Ricerche - Unit of Bologna*
Via Gobetti, 101, I-40129, Bologna, Italy
[*]*corresponding author: sandro.rao@unirc.it*

Abstract: Electro optical absorption in hydrogenated amorphous silicon (α-Si:H) – amorphous silicon carbonitride (α-SiC_xN_y) multilayers have been studied in two different planar multistacks waveguides. The waveguides were realized by plasma enhanced chemical vapour deposition (PECVD), a technology compatible with the standard microelectronic processes. Light absorption is induced at λ = 1.55 μm through the application of an electric field which induces free carrier accumulation across the multiple insulator/ semiconductor device structure. The experimental performances have been compared to those obtained through calculations using combined two-dimensional (2-D) optical and electrical simulations.

OCIS codes: (130.4110) Modulators; (130.3120) Integrated optics devices; (160.2100) Electro-optical materials.

References and links

1. R. A. Soref, "Silicon-based optoelectronics," in Proc. IEEE **81**, 1687–1706 (1993).
2. G. T. Reed and A. P. Knights, "Silicon Photonics: An Introduction," Wiley, New York (2004).
3. G. Cocorullo, M. Iodice, I. Rendina, P.M. Sarro, "Silicon thermo-optical micromodulator with 700 kHz 3dB bandwidth," IEEE Photon. Technol. Lett. **7**, 363-365 (1995).
4. A. Liu, R. Jones, L. Liao, D. Samara-Rubio, D. Rubin, O. Cohen, R. Nicolaescu M. Paniccia, "A high-speed silicon optical modulator based on a metal-oxide-semiconductor capacitor," Nature **427**, 615-618 (2004).
5. A. Liu, L. Liao, D. Rubin, H. Nguyen, B. Ciftcioglu, Y. Chetrit, N. Izhaky M. Paniccia, "High-speed optical modulation based on carrier depletion in a silicon waveguide," Opt. Express **15**, 660-668 (2007).
6. D. Marris-Morini, X. Le Roux, L. Vivien, E. Cassan, D. Pascal, M. Halbwax, S. Maine, S. Laval, J. M. Fédéli, J. F. Damlencourt, "Optical modulation by carrier depletion in a silicon PIN diode," Opt. Express **14**, 10838-10843 (2006).
7. G. V. Treyz, P. G. May J. M. Halbout, "Silicon Optical Modulators a 1.3 μm based on Free Carrier Absorption," IEEE Electron Device Lett. **12**, 276-278 (1991).
8. A. Sciuto, S. Libertino, S. Coffa, G. Coppola, "Miniaturizable Si-based electro-optical modulator working at 1.5 μm," Appl. Phys. Lett. **86**, 20115 (2005).
9. T. Tabei, Tomoki Hirata, K. Kajikawa, H. Sunami, "Potentiality of Silicon Optical Modulator Based on Free-Carrier Absorption," IEEE International Electron Devices Meeting, pp. 1023-1026 (2007).
10. G. Cocorullo, F. G. Della Corte, I. Rendina, "Amorphous silicon waveguides and light modulators for integrated photonics realized by low-temperature plasma-enhanced chemical-vapor deposition," Opt. Lett. **21**, 2002-2004 (1996).
11. M. Okamura, S. Suzuki, "Infrared photodetection using α-Si:H photodiode," IEEE Photon. Technol. Lett. **6**, 412–414 (1994).
12. G. Cocorullo, F.G. Della Corte, R. De Rosa, I. Rendina, A. Rubino, E. Terzini, "Amorphous silicon-based guided-wave passive and active devices for silicon integrated optoelectronics," IEEE J. Quantum Electron **4**, 997–1001 (1998).

#93745 - $15.00 USD Received 11 Mar 2008; revised 23 Apr 2008; accepted 29 Apr 2008; published 9 May 2008

13. B.Han, R.Orobtchouk, T.Benyattou, P.R.A. Binetti, S. Jeannot, J. M. Fedeli, X.J.M. Leijtens, "Comparison of optical passive integrated devices based on three materials for optical clock distribution," in Proc. ECIO 07, Copenhagen, Denmark, pp. 1-4 (2007).
14. F.G. Della Corte, M. Gagliardi, M. A. Nigro, C. Summonte "In-guide pump and probe characterization of photoinduced absorption in hydrogenated amorphous silicon thin films," J. Appl. Phys. **100**, 033104 (2006).
15. M. Zelikson, K. Weiser, A. Chack, J. Kanicki, "Direct determination of the quadratic electro-optic coefficient in an α-Si:H based waveguide," Jour. Non Cryst. Sol. **198-200**, 107-110 (1996).
16. RSoft Photonics CAD Layout User Guide, Rsoft Design Group, Inc. Physical Layer Division, 200 Executive Blvd. Ossining, NY 10562.
17. E. Centurioni, "Generalized matrix method for calculation of internal light energy flux in mixed coherent and incoherent multilayers," Appl. Opt. **44**, 7532-7539 (2005).
18. W. B. Jackson, N. M. Amer, A. C. Boccara, D. Fournier, "Photothermal deflection spectroscopy and detection," Appl. Opt. **20**, 1333 (1981).
19. G. Lavareda, C. Nunes de Carvalho, E. Fortunato, A. Amaral, A.R. Ramos, "Properties of α-Si:H TFTs using silicon carbonitride as dielectric", Jour. Non Cryst. Sol. **338–340**, 797–801 (2004).
20. C. A. Barrios, "Electrooptic Modulation of Multisilicon-on-Insulator Photonic Wires," Journal of Lightwave Technology **24**, 2146-2155 (2006).
21. T. S. Moss, G. J. Burrell, B. Ellis, "Semiconductor Opto-Electronics," London Butterwoth, (1973).
22. G. Cancellieri, U. Ravaioli, "Measurements of Optical Fibers and Devices: Theory and Experiments", Dedham MA, Artech House (1984).
23. R. A Street, "Hydrogenated Amorphous Silicon," Cambridge University Press (1991).
24. K. Fukuda, N. Imai, S. Kavamura, K. Matsumura, N. Ibaraki, "Switching performance of high rate deposition processing α-Si:H TFTs," Jour. Non Cryst. Sol. **198-200**, 1137-1140 (1996).
25. Y. Chen, S. Wagner, "Inverter made of complementary *p* and *n* channel transistors using a single directly deposited microcrystalline silicon film," Appl. Phys. Lett. **75**, 1125 (1999).
26. A. Z. Kattamis, R. J. Holmes, I-Chun Cheng, Ke Long, J. C. Sturm, S. R. Forrest, and Sigurd Wagner, "High mobility nanocrystalline silicon transistors on clear plastic substrates," IEEE Electron Device Lett. **27**, 49-51 (2006).
27. M.N. Troccoli, A. J. Roudbari, T. Chuang, M. K. Hatalis, "Polysilicon TFT circuits on flexible stainless steel foils," Solid-State Electronics **50**, 1080-1087 (2006).
28. ATLAS device simulation software user's manual, SILVACO Int., Santa Clara, CA, (2005).
29. J. Singh, "Effective mass of charge carriers in amorphous semiconductors and its applications," Jour. Non Cryst. Sol. **120**, 295-300 (1973).
30. F.G. Della Corte, A. Rubino, G. Cocorullo, "Simulation study and realisation of an α-Si:H emitter on GaAs," Solid-State Electronics **42**, 1819-1825 (1998).

1. Introduction

In recent years, silicon microphotonic circuits have generated great interest [1], and on-chip optical links are nowadays considered a promising alternative to electrical interconnects due to their bandwidth, consumption, noise, crosstalk and data throughput implications. Thanks to its cheap and well established technology, crystalline silicon (c-Si) is an ideal candidate for such applications in the near infrared region, and an ample volume of work exists in the field [2].

In order to develop Si-based active photonic systems, several characteristic optical effects present in this semiconductor have been exploited, among which the thermo-optic effect [3] and free-carrier related electro-optic effects on the real part [4, 5, 6] and on the imaginary part [7, 8, 9] of the refractive index.

However, one of the main concerns about these devices is their actual compatibility, at minimum or no costs, with the as wide as possible CMOS process portfolio offered by silicon foundries. For this reason, the definition of a low-impact technology, allowing the fabrication of a photonic layer on top of every microchip, would be of particular importance.

Hydrogenated amorphous silicon (α-Si:H) also shows interesting features which make it attractive for lightwave communication purposes: it is transparent in the infrared [10], exhibits refractive index tunability by acting on the process parameters, and has a very good technological compatibility with microelectronics, due in particular to the low thermal budget

#93745 - $15.00 USD Received 11 Mar 2008; revised 23 Apr 2008; accepted 29 Apr 2008; published 9 May 2008

involved in its deposition and structuring, which can take place at T<250 °C, *e.g.* at the end of the CMOS process flow. Applications have been already proposed for this material in the optical communication area for the detection of photons [11], and for lightwave guiding [12 13].

Thermo-optical and all-optical effects have also been exploited in α-Si:H to demonstrate modulation or switching action in planar devices for integrated photonics [12, 14]. Electro-optical effects, in contrast, have been rarely considered in this material due to the weak incidence of electric field on the refractive index [15], on one side, and the difficulty of reaching a significant carrier injection across p-n junctions in amorphous semiconductors, on the other side.

In this paper we report results on a field effect induced light modulation at $\lambda = 1.55$ μm in α-Si:H/α-SiCN multi-stack planar waveguiding structures deposited by PECVD on a c-Si substrate. The modulation mechanism has been modelled as a free carrier effect on the imaginary part of the refractive index. In particular, the absorption is enhanced by carrier accumulation at the intermediate semiconductor/insulator interfaces. The carrier profile under bias was estimated by means of electrical simulations and used for optical simulations. The results are found to be in agreement with the experimental data.

2. Design and fabrication

We designed and fabricated two different waveguides, whose cross sections are sketched in Fig. 1. The first waveguide consists of the stack of three bi-layers each composed of a 1 μm-thick α-Si:H layer and a 30 nm-thick α-SiCN layer, deposited on a <100> heavily doped silicon substrate. The substrate and the stack are separated by a 0.39 μm-thick Si_3N_4 low refractive index cladding layer. The second waveguide differs from the first one only in that it is made of six stacked bi-layers each composed of a 0.5 μm-thick α-Si:H layer and a 40 nm-thick α-SiCN layer. The waveguide thickness is 3.5 μm approximately in both cases, in order to maximize the coupling with the 3 μm wide spot of our lensed fibers.

Due to the steep change in the refractive indices of α-Si:H and Si_3N_4, $\Delta n \approx 2$, a strong vertical confinement is achieved. A 100 nm-thick transparent conductive Indium Tin Oxide (ITO) thin film forms the top contact, while the bottom contact is the Si substrate itself.

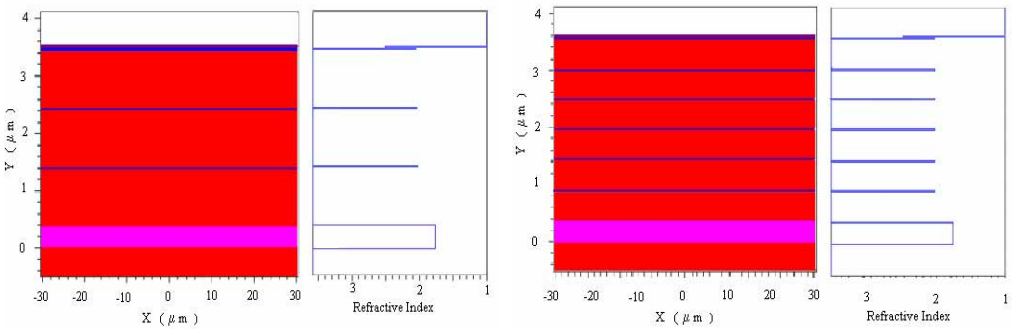

Fig. 1. Schematic cross sections of the realised planar waveguides and corresponding refractive index profiles. The crystalline silicon substrate is 300 μm thick.

The propagation characteristics of the waveguides were studied by means of a numerical electromagnetic-wave solver based on the Beam Propagation Method (BPM) [16]. The optical data on the materials, used for simulations, were determined from the analysis of the experimental transmittance and reflectance spectra, in the wavelength range 0.5 to 2 μm, of test films deposited on Corning glass. The reflectance-transmittance analysis tool OPTICAL [17] was used for this analysis, which also allowed determining the layer thicknesses. Photothermal deflection spectroscopy (PDS) [18] was used to determine the absorption

#93745 - $15.00 USD Received 11 Mar 2008; revised 23 Apr 2008; accepted 29 Apr 2008; published 9 May 2008

coefficient at 1.55 μm. Conductivity measurements were also performed using a computer controlled parametric characterization system based on an automatic probing station. These measurements were performed at room temperature in the dark. The fundamental process parameters and material characteristics at λ = l.55 μm are listed in Table 1.

For both waveguides, the simulator predicts that single mode operation is obtained once a 10 μm wide rib is defined by fully etching the 100 nm thick ITO top layer. Figures 2 and 3 show the fundamental TE_0 and TM_0 modes, respectively characterized by propagation losses of 2.1 dB/cm and 2.5 dB/cm for the three bi-layer waveguide, and 2.1 and 7.1 dB/cm for the six bi-layer waveguide.

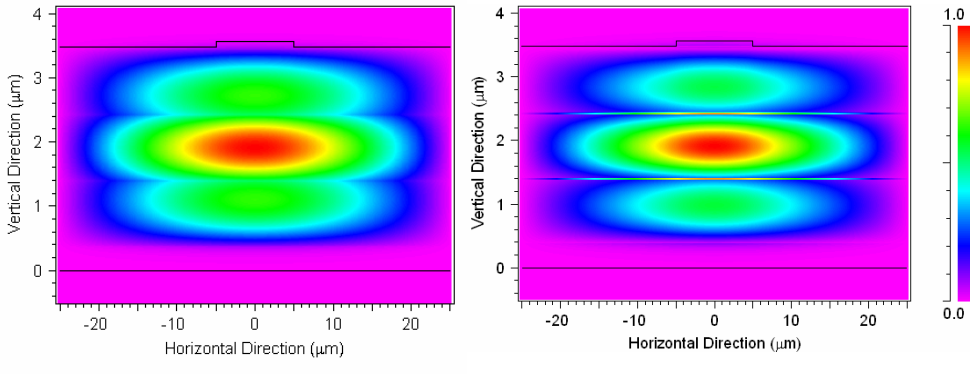

Fig. 2. TE (left) and TM (right) fundamental optical mode-field profiles of the three bi-layer waveguide.

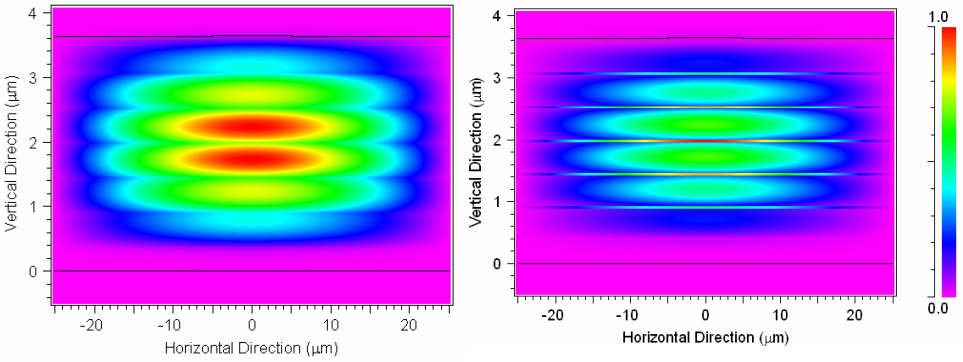

Fig. 3. TE (left) and TM (right) fundamental optical mode-field profiles of the six bi-layer waveguide.

Both waveguide structures exhibit a dominant single-mode operation for TE and TM polarization modes. BPM calculations of the first-order higher mode TE_{01} and TM_{01} show that there is negligible optical field in the waveguide core for these modes and the highest values of the field are localized in the slabs, far from the core. Thus, the TE_{01} and TM_{01} modes are vanishing modes, while the fundamental TE and TM mode are the only confined modes.

A better lateral confinement could be obtained with a higher rib, which would however require the dry etching of the α-Si:H/α-SiNC stack. We have calculated, for instance, that a 5 μm wide and 0.4 μm high rib would allow single mode propagation in both waveguide types, with 90% of the radiation extending, in the horizontal direction, less than 5 μm from

#93745 - $15.00 USD Received 11 Mar 2008; revised 23 Apr 2008; accepted 29 Apr 2008; published 9 May 2008

waveguide the center. This would also improve the bend losses that may arise in more complex devices.

The fabrication of the three bi-layer waveguide begins with a surface cleaning treatment, using H_2SO_4+H_2O_2 and HF solutions on the n-type highly doped c-Si substrate (ρ=0.001 Ω·cm). The substrate is then loaded into the four-chamber RF (13.56 MHz) system. First, the Si_3N_4 cladding layer is deposited from the plasma-assisted decomposition of SiH_4 and NH_3, at a RF power P_{RF} = 4W. Subsequently, the first α-Si:H layer is deposited in SiH_4 atmosphere, followed by the deposition of the α-SiCN layer from a gaseous mixture of SiH_4, NH_3 and CH_4. The forth / fifth and sixth / seventh deposition steps are made under the same conditions as the second / third ones. Temperature is 220°C for all steps. The 100 nm-thick top ITO film is deposited by magnetron sputtering. The 10 μm-wide, fully etched ITO rib was obtained by photolithographic patterning and wet etching in 5% HCl solution. The fabrication of the six bi-layer waveguide followed the same procedure, although with scaled deposition times.

Table 1. PECVD process parameters for the three bi-layer device: frequency, power, pressure, substrate temperature, time. For the thinner six bi-layer device the deposition times are scaled accordingly. Refractive index *n* and absorption coefficient α are measured at 1.55 μm. Process gas flows measured in Standard Cubic Centimetres per Minute (sccm).

Material	RF (MHz)	Power (W)	Pressure (hPa)	T (°C)	time (h mm ss)	Process Gas (sccm)			*n*	*a* (cm^{-1})	σ (S/cm)
Si_3N_4	13.56	4	0.8	220	26’	SiH_4	NH_3		1.77±0.02	2.30±50%	$< 10^{-16}$
						1.5	68				
α-Si:H	13.56	4	0.53	220	1^h48’20”	SiH_4			3.58±0.02	0.33±50%	$2.6\ 10^{-9}$
						20					
α-SiCN	13.56	4	0.53	220	3’05”	SiH_4	NH_3	CH_4	2.03±0.02	0.69±50%	$5.2\ 10^{-16}$
						8	24	8			

In our devices the thin α-SiCN highly insulating layers break the conduction between the α-Si:H films so that the device electrically behaves as a series of capacitors. The ternary alloy SiC_XN_Y has in fact good insulating properties and forms good interfaces with amorphous silicon. For this reason it has been exploited as the dielectric layer in α-Si:H thin film transistors (TFTs) in place of the traditional SiN_X gate insulator [19].

The application of a voltage across the stack therefore produces an accumulation of electrons and holes respectively at the opposite sides of each insulating film, and therefore at intermediate depths across the waveguide. This approach has been theoretically proven to enhance the effects induced by free carriers on the optical propagation characteristics of c-Si waveguides [20].The thickness of the α-SiCN was therefore chosen as thin as possible in order to preserve the optical propagation characteristics of the waveguide, but nevertheless thick enough to avoid dielectric perforation when a potential of the order of 10 V is applied across. We consider 30-40 nm a good trade off in respect.

3. Experimental

The principle used to modulate the light signal is the variation of the free carrier concentration at the multiple α-Si:H/α-SiCN interfaces. The Si refractive index and absorption coefficient depend on the free carrier concentration by the dispersion relation [21] that can be derived, to a first order approximation, from the classical Drude model:

#93745 - $15.00 USD Received 11 Mar 2008; revised 23 Apr 2008; accepted 29 Apr 2008; published 9 May 2008

$$\Delta n = -\frac{e^2\lambda^2}{8\pi^2 c^2 \varepsilon_0 n}\left(\frac{\Delta N_e}{m_e} + \frac{\Delta N_h}{m_h}\right) \quad (1)$$

$$\Delta\alpha = \frac{e^3\lambda^2}{4\pi^2 c^3 \varepsilon_0 n}\left(\frac{\Delta N_e}{m_e{}^2\mu_e} + \frac{\Delta N_h}{m_h{}^2\mu_h}\right) \quad (2)$$

where Δn and $\Delta\alpha$ are the variations of the real part of the refractive index (n) and of the absorption coefficient (α) due to the free carrier concentration change, e is the electron charge, ε is the permittivity in free space, n is the refractive index of intrinsic Si, μ is the free carrier mobility, m is the effective mass, ΔN is the free carrier concentration variation, and λ is the wavelength. The subscripts e and h refer to electrons and holes, respectively.

The presence of the α-SiCN thin film between two layers of α-Si:H creates a capacitive device. The effect of the introduction of the α-SiCN regions is therefore a distribution of the excess free carriers across the device section, and consequently an enhancement of the modulation efficiency. In our experiments a 15 mW laser beam (λ = 1.55 μm) was sent, with no polarization control, over a 8 μm core monomode fiber, and coupled at its opposite lensed end to the waveguide core. The ITO top rib was effective in reducing the lateral in-plane divergence. The transmitted light was collected at the chip output by a 50 μm core multimode fiber and detected by an InGaAs photodiode. Great care was taken to prevent stray light passing above the sample.

The waveguide propagation losses were first measured by the cut-back technique [22]. Several samples with lengths in the range 0.5 cm to 1.5 cm were cut from the substrate by cleavage. Sample facets did not receive polishing treatment. From these samples we calculated a loss coefficient of 2.25±0.03 dB/cm for the three-layers waveguide and 2.77±0.09 dB/cm for the six-layers waveguide, which are close to those estimated by simulations. The overall insertion losses of the devices are above 11 dB, with the main contribution due to the coupling losses, a drawback of the high refractive index of silicon used as the core material. We believe that a reduction of the propagation losses can be obtained through a finer tuning of the multi-stack deposition process, aiming in particular at a tighter control of the α-Si:H defect states [10]. A set of four samples were used to characterize the modulation effect by applying square voltage pulses to the electrodes. The detector output was fed into a lock-in amplifier so that changes in the transmitted light intensity, ΔI, could be measured synchronously with the voltage pulses. We measured the modulation depth, defined as:

$$M = \frac{I_{MAX} - I_{MIN}}{I_{MAX}} \quad (3)$$

where I_{MAX} and I_{MIN} are the maximum and minimum intensities of the transmitted signal.

Figure 4 reports the dependence of M on the modulating signal amplitude at a frequency of 10Hz and a duty cycle of 50%.

A maximum modulation depth up to 9% is obtained for the three bi-layer sample (L=1.2 cm), while a maximum modulation depth of 27% is obtained for the 1.5 cm long, six bi-layer, sample.

#93745 - $15.00 USD Received 11 Mar 2008; revised 23 Apr 2008; accepted 29 Apr 2008; published 9 May 2008

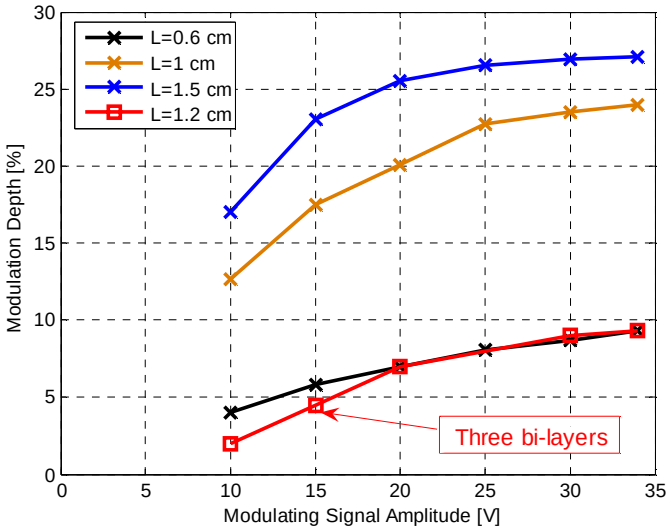

Fig. 4. Dependence of *M* on the modulating signal amplitude for three and six bi-layer samples.

The reported data show that *M* increases with the modulating signal amplitude and with the device lenght. The average effective absorption coefficient variation $\Delta\alpha_{eff}$ induced in the six bi-layer waveguide is 0.11, 0.18 and 0.21 cm^{-1} respectively at 10, 20 and 30 V biases, corresponding to an electric field of 0.15, 0.30 and 0.45 MV/cm across the 40 nm-thin insulating α-SiCN layers. An enhancement of the modulation performance, *e.g.* of an order of magnitude on $\Delta\alpha_{eff}$, thus allowing the design of effective active devices, could be obtained through an increase of the number of the α-Si:H/α-SiNC bi-layers in the stack and a thinning of the stack, as both approaches would in fact increase the relative volume of the waveguide where carrier accumulation takes place. This would also allow using lower bias voltages to obtain comparable modulation performances.

Figure 5 shows the output light power and the applied voltage as a function of time for the six bi-layer, 1 cm long, waveguide for 15 V amplitude applied pulses.

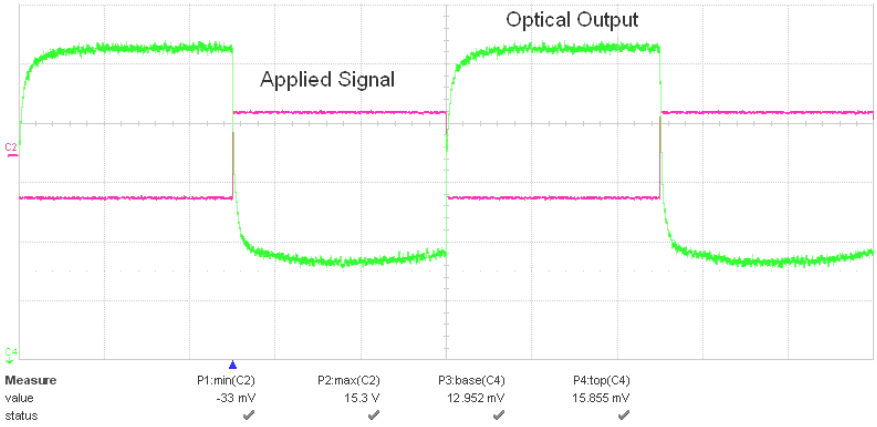

Fig. 5. Output light power and applied voltage for a six bi-layer 1 cm long waveguide. The modulating signal has V_{min}=0 V, V_{max}=15 V, duty-cycle=50%, frequecy=10Hz.

It is worthwhile noting that the application of an electric bias across all of the devices always produced a reduction of the transmittance, an observation allowing to conclude that,

#93745 - $15.00 USD Received 11 Mar 2008; revised 23 Apr 2008; accepted 29 Apr 2008; published 9 May 2008

because of the poor quality of the facets, none of the samples behaved as a Fabry-Perot resonator. As a further support to this conclusion, no evidence of thermo-optic modulation [10] in the transmitted signal was observed after the application of smooth temperature changes in the range ± 2°C. Therefore we can assume that the reported measurements are not affected by a change in the real part of the refractive index. However, a modification of the absorption coefficient is certainly associated to a modification of *n*, an effect that, once characterized, could be advantageously exploited for the design of phase shift based devices, *e.g.* in a Mach-Zehnder interferometer.

The *M* vs. frequency plot is shown in Fig. 6 for the 1 cm-long, six bi-layer device, driven by 20V pulses. The modulation bandwidth is limited by the characteristic times of the carrier trapping and releasing phenomena involving the shallow levels in the disordered α-Si:H films [23]. In fact, at every change of the applied electrical bias in either direction, a transient takes place during which either part of the carriers slowly recombine, if the bias is reducing, or newly generated carriers are slowly accumulated, if the bias is increasing. We believe however that the switching performances can be improved. As a first reference, cut-off frequencies of about 1 MHz have been reported for the charge density modulation in the channel of TFT's based on α-Si:H films [24]. Better results can be expected in nano or micro-crystalline Si films which, deposited at low temperatures as well, indeed perform several order of magnitude lower trap concentrations with respect to α-Si:H, and therefore better transport characteristics [25, 26]. Finally, switching performances above 1 GHz have been reported for TFT's made in polycrystalline Si, initially deposited at low temperature in the amorphous phase and then crystallized by laser annealing [27].

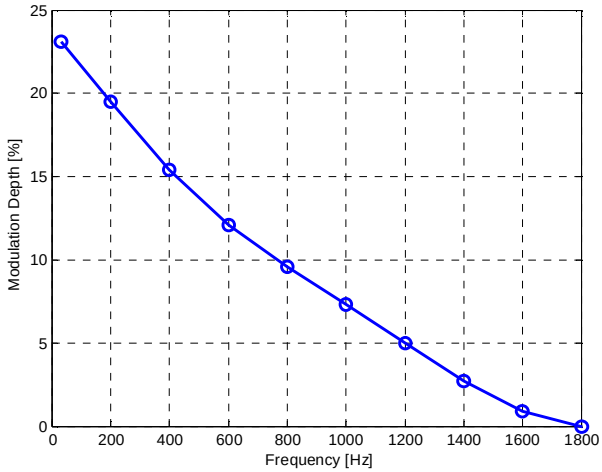

Fig. 6. Modulation depth vs. Frequency. The modulating signal voltage amplitude for the six bi-layer, 1-cm-long waveguide is V=20V, duty-cycle=50%.

As no other active optical devices are know in α-Si:H exploiting electrically induced free carrier effects, the features of the presented devices can be compared to those of other known absorption-type modulators in crystalline silicon, like for instance those proposed in Refs. [7, 8, 9]. The first device exploits bipolar carrier injection, and requires current densities of about 2 kA/cm^2 to get an absorption coefficient variation $\Delta\alpha$ of 5 cm^{-1}. The more recent device of Ref. [8] performed a $\Delta\alpha$ better than 100 cm^{-1} at comparable current densities. In both cases, however, the high current might be responsible of a heating and a thermal drift of the devices, requiring appropriate cooling systems. The device proposed in Ref. [9] is embedded in a MOS structure. In this case the dissipated power, both static and dynamic, can be considered negligible. The modulator, which is 5 mm long, performs a 0.95 dB extinction ratio,

#93745 - $15.00 USD Received 11 Mar 2008; revised 23 Apr 2008; accepted 29 Apr 2008; published 9 May 2008

corresponding to a $\Delta\alpha \approx 0.4$ cm^{-1}, for an applied electric field across the oxide of approximately 3.6 MV/cm, well above the electric field considered in our experiments.

4. Numerical simulations

As already mentioned, from an electrical point of view the proposed structures, made of alternate layers of α-Si:H and α-SiCN, in fact behave as the series of capacitors. The application of a biasing voltage between the ITO layer and the substrate determines an accumulation of holes and electrons at the opposite ends of each internal α-SiCN insulating layer.

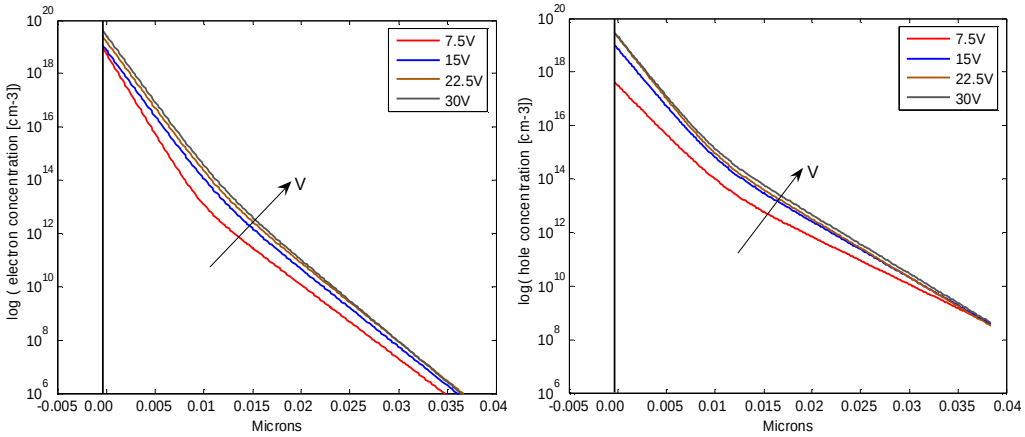

Fig. 7. Electron (left) and hole (right) concentration depth profiles calculated in the α-Si:H layer close to the α-Si:H/α-SiCN interface. The applied biases are from 1.5 V to 30 V.

In order to model the modulation effect, a mixed electrical-optical simulation study was performed.

The carrier distributions under bias were first determined by carrying out electrical simulations with a finite element Computer Aided Design code specifically designed for the simulation of solid-state devices including amorphous semiconductor regions, *ATLAS-TFT* [28]. Simulation parameters were set as reported in Table 2 and Refs. [29, 30]. With a maximum grid spacing of 1 nm in the accumulation regions, we calculated the excess electrons and holes at each α-Si:H/α-SiCN interface. As an example, we report in Fig. 7 the electron and hole concentration depth profiles for the three bi-layer device, calculated close to the central α-Si:H/α-SiCN interfaces, for total applied biases across the device ranging from 7.5V to 30V.

Table 2. Physical parameters used for the α-Si:H layer for the electrical simulations.

E_g (eV)	μ_n (cm^2/V·s)	μ_p (cm^2/V·s)	m_n^* (Kg)	m_h^* (Kg)	m_0 (Kg)	χ (eV)	$E_{G,C}$ (eV)	$E_{G,V}$ (eV)
1.8	0.1	0.01	$0.34 \cdot m_0$	$0.34 \cdot m_0$	$3.09\ 10^{-31}$	4.1	0.83	0.58

These profiles were subsequently used to calculate, through Eq. (2), the absorption profiles provided to the optical simulator, using the same grid spacing. The study was limited however to the three bi-layer device, as the modelling of the six-layers device in the absorbing

#93745 - $15.00 USD Received 11 Mar 2008; revised 23 Apr 2008; accepted 29 Apr 2008; published 9 May 2008

phase often resulted in non-converging solutions, either for the electrical or for the optical simulation tools.

The calculated modulation depths *M*, both for the TE_0 and TM_0 modes, are shown in Fig. 8 together with the experimental data. This plot shows that the modulation effect is rather strongly polarization sensitive, while the fact that the experimental modulation, obtained for unpolarized radiation, falls within the theoretical limits is an element in favour of the assumed device physics.

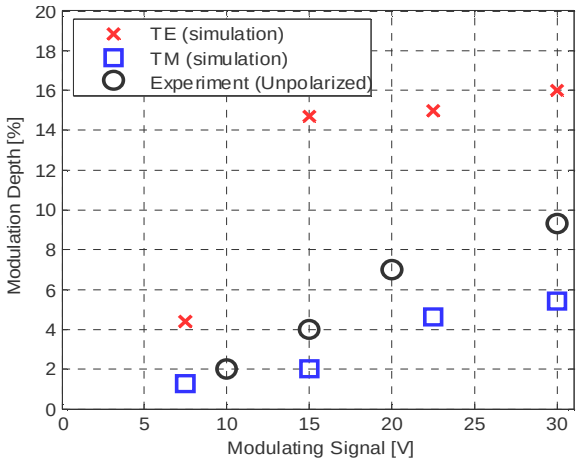

Fig. 8. Comparison of *M* at various modulating signal amplitudes: TE_0, TM_0, Experimental data (unpolarized input), for the three bi-layer sample.

A validation of the estimated overall charge accumulation used in Eqs. (1) and (2) was obtained by comparing the experimental capacitance of the stack with that obtained through calculations.

With a precision LCR meter (20Hz - 1MHz), the device capacitance was measured in the low frequency region (experimental points in Fig. 9). This plot shows that the capacitance sharply increases with decreasing frequencies. This phenomenon has to be correlated to the fact that, by lowering the frequency, an increasing number of carriers are involved for each cycle in the trapping and releasing processes taking place in the disordered α-Si:H. To circumvent this effect, which can also induce faulty results in dynamic simulations, the quasi-static capacitance C(ω=0) was extrapolated from this graph. In the same figure the best fittings obtained for three different fitting curves are also shown. Table 3 summarizes the fitting functions and the corresponding RMS errors. The best fitting is obtained with the two-exponential function, which allows extrapolating a capacitance of approximately 9 nF/cm^2 at ω=0 . Since our device is the series of three equal capacitors, the capacitance across one α-Si:H/α-SiCN/α-Si:H stack is assumed to be 27 nF/cm^2.

Table 3. Fitting functions and corresponding RMS errors

Fitting Function	a	b	c	d	RMS Error
ax^3+bx^2+cx+d	-5.85×10^{-7}	2.98×10^{-4}	-5.06×10^{-2}	4.07	0.29
$a\cdot\exp(bx)$	3.36	-6.97×10^{-3}	--	--	0.36
$a\cdot\exp(bx)+c\cdot\exp(dx)$	6.91	-7.35×10^{-2}	2.06	-3.25×10^{-3}	0.13

At the same time the static capacitance ΔQ/ΔV was estimated from the carrier profiles calculated by the simulator. By integrating the calculated carrier concentration profiles in α-

#93745 - $15.00 USD Received 11 Mar 2008; revised 23 Apr 2008; accepted 29 Apr 2008; published 9 May 2008

Si:H at the two biases of 10 and 15 V across one α-Si:H/α-SiCN/α-Si:H stack (Fig. 7), we calculated the total differential capacitance, obtaining C ≈ 26.5 nF/cm^2, in good agreement with the measured value.

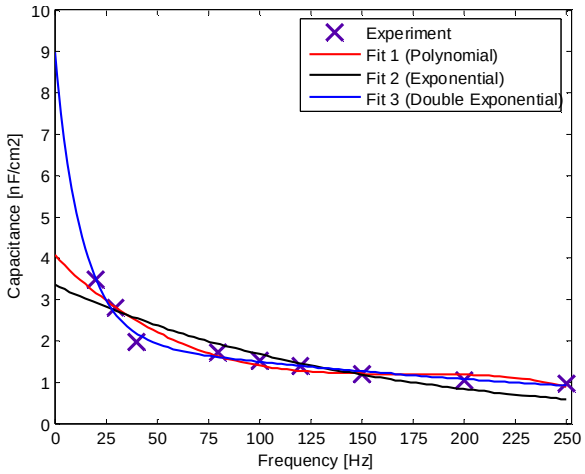

Fig. 9. Experimental dependence of the three bi-layer device capacitance on frequency and its best fittings through three fitting functions.

5. Conclusion

Two multi-stack structures, based on the CMOS-compatible technology of amorphous silicon, have been explored for enhancing electro-optical modulation effects in integrated, waveguide embedded, photonic devices.

The single mode waveguiding structures, consisting of three (six) α-Si:H/α-SiCN stacks deposited by PECVD on a c-Si substrate, were realized and characterized. They showed propagation losses of 2.25 (2.77) dB/cm at the wavelength of 1.55 μm. The application of an external electric field across the structure produces carrier accumulation at the intermediate semiconductor/insulator interfaces, which is in turn responsible of an enhanced optical absorption. We measured a $\Delta\alpha_{eff}$ of 0.21 cm^{-1} when an electric field of 0.45 MV/cm is applied across each α-SiCN dielectric thin film.

The experimental data were interpreted by means of mixed electrical-optical simulations, which allowed calculating, at several bias points, the accumulated carrier profiles and the free carrier induced optical absorption variations. We found a good agreement between the simulated and experimental optical modulation of the device.

As an additional support to the proposed modulation model, a good agreement was found between the estimated quasi-static capacitance of the device and the experimental one, leading to conclude that the electrical parameters used for simulations allow the correct estimation of the accumulated carriers.

Technologically, the fabrication process involves temperatures under 220°C, which are compatible with the standard microelectronic processes and in particular suitable for the realization of a photonic layer on top of an integrated circuit.

Acknowledgment

IMM-CNR, Unit of Napoli (Italy), where the optical simulations were performed, is gratefully acknowledged.

#93745 - $15.00 USD Received 11 Mar 2008; revised 23 Apr 2008; accepted 29 Apr 2008; published 9 May 2008